not continuous as in the bulk but are discrete, due to the confinement of the electron wavefunction to the physical dimensions of the particles [4]. This phenomenon is called *quantum confinement*; therefore, nanocrystals are also known as quantum dots. In other words, a small nanocrystal could be a very bad conductor, although nanocrystals are tiny silhouettes of the conducting bulk. Likewise, a tiny nanocrystal of a ferromagnet can be paramagnetic in nature. In several respects, small nanocrystals behave like molecules. The nanocrystals can be discretely charged with electrons with characteristic charging energies. This means that a nanocrystal carrying an extra electron can exhibit properties different from those of a neutral species.

The shrinking dimensions of the current microelectronic devices and the realization that current lithographic processes cannot extend to the nanoworld [5] have lent tremendous thrust to research aimed at ordering nanocrystals into functional networks [6–11]. The nanocrystals akin to covalent systems self-assemble into ordered arrays in one, two, and three dimensions under the right conditions. Lattices of nanocrystals consist of interacting nanocrystals and may exhibit novel properties arising out of such interactions. Thus, the ability to engineer such assemblies extends the reach of current lithographic techniques and holds promise for a new generation of electronics of the nanoworld [6]. In this context, synthesis and programmed assembly of nanocrystals assume significance.

In this chapter we discuss the physical and chemical properties of metal nanocrystals, with emphasis on size-dependent properties. The ability of nanocrystals to form mesoscopic organizations in one, two, and three dimensions is also examined. Collective properties of nanocrystal organization are presented.

2. SYNTHETIC STRATEGIES

2.1. General Methods

Chemical synthesis of sols of metals results in nanoparticles embedded in a layer of ligands or stabilizing agents, which prevent the aggregation of particles. The stabilizing agents employed include surfactants such as long-chain thiols or amines or polymeric ligands such as polyvinylpyrrolidone (PVP). Reduction of metal salts dissolved in appropriate solvents produces small metal particles of varying size distributions [12–15]. A variety of reducing agents have been employed for reduction. These include electrides, alcohols, glycols, metal borohydrides, and certain specialized reagents such as tetrakis(hydroxymethyl) phosphonium chloride.

Successful nanocrystals synthesis has also been carried out employing soft templates such as the water pool in a reverse micelle, the interface of two

phases. Reverse micellar methods have been successfully utilized in the preparation of Ag, Au, Co, Pt, and Co nanocrystals [16, 17]. The synthesis of nanocrystals at the air–water interface as in Langmuir–Blodgett films or at a liquid–liquid interface is currently attracting wide attention [7, 18, 19]. It has been shown recently that films of metal, semiconductor, and oxide nanocrystals can be prepared using a water–toluene interface [20, 21]. A typical film of Au nanocrystals is shown in Figure 1.1. Traditionally, clusters of controlled sizes have been generated by abalation of a metal target in vacuum followed by mass selection of the plume to yield cluster beams [22, 23]. Such cluster beams could be subject to *in situ* studies or be directed on to solid substrates. In order to obtain nanocrystals in solution, Harfenist et al. [24] steered a mass-

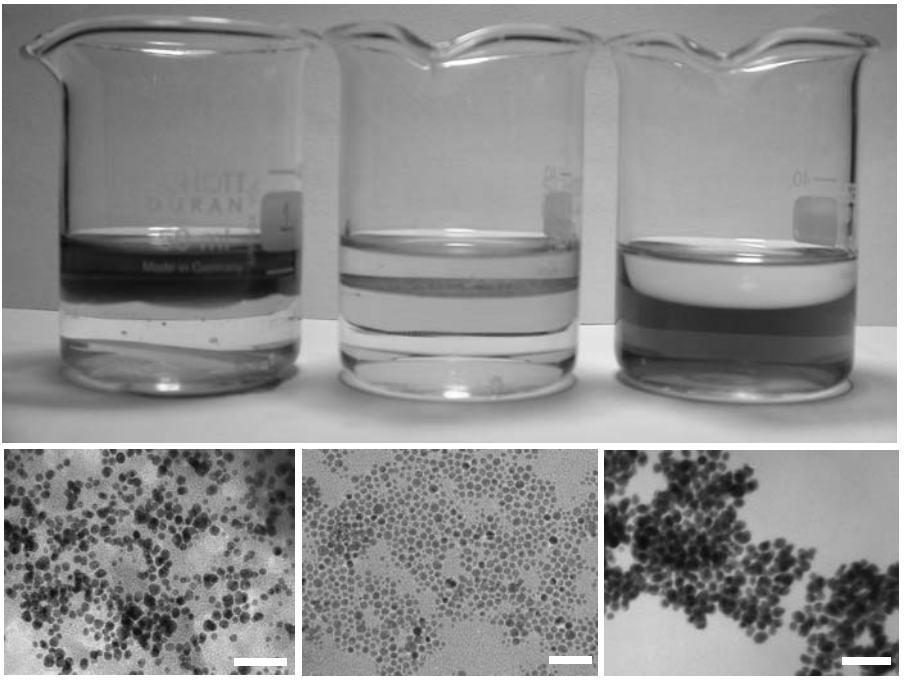

Figure 1.1. Nanocrystalline film of Au formed at the toluene–water interface (**middle**). Gold is introduced as a toluene solution of $Au(PPh_3)Cl$ while partially hydrolyzed THPC [tetrakis(hydromethyl) phosphonium chloride] in water acts as a reducing agent. The film is obtained when the two layers are allowed to stand for several hours. When dodecanethiol is added to the toluene layer, the film breaks up forming an organosol (**left**) while mercaptoundecanoic acid added to water produces a hydrosol (**right**). Shown below are the corresponding TEM images showing nanocrystals. The scale bars correspond to 50 nm.

selected Ag cluster beam through a toluene solution of thiol and capped the vacuum-prepared particles.

Colloids of alloys have been made by the chemical reduction of the appropriate salt mixture in the solution phase. In the case of semiconductor nanocrystals, a mixture of salts is subject to controlled precipitation. Thus, Ag–Pd and Cu–Pd colloids of varying composition have been prepared by alcohol reduction of mixtures of silver nitrate or copper oxide with palladium oxide [25]. Fe–Pt alloy nanocrystals have been made by thermal decomposition of the Fe and Pt acetylacetonates in high-boiling organic solvents [26]. Au–Ag alloy nanocrystals have been made by co-reduction of silver nitrate and chloroauric acid with sodium borohydride [27, 28]. Au–Ag alloying and segregation has been brought about by the use of lasers on Au–Ag-layered particles [29, 30].

2.2. Size Control

The successful synthesis of nanocrystals involves three steps: nucleation, growth, and termination by the capping agent or ligand [12–14]. Though the reaction temperature and reagent concentrations provide a rudimentary control of the three steps, it is often impossible to independently control them and so the obtained nanocrystals usually exhibit a distribution in size. Typically, the distribution is log-normal with a standard deviation of 10% [14]. Given the fact that properties of the nanocrystals are size-dependent, it is significant to be able to synthesize nanocrystals of precise dimensions with minimal size distributions. This can be accomplished to a limited extent by size-selective precipitation either by centrifugation or by use of a miscible solvent–nonsolvent liquid mixture to precipitate nanocrystals. Schmid [31] and Zamaraev and co-workers [32] succeeded in preparing truly monodisperse nanocrystals that they called "cluster compounds." These cluster compounds are like macromolecules with a core containing metal–metal bonds, yet they are obtainable in definite stoichiometries, with typical examples being $[Pt_{38}(CO)_{44}H_2]^{2-}$ and $Au_{55}(PPh_3)_{12}Cl_6$. The enhanced stability of Au_{55} was recently demonstrated clearly by Boyen et al. [33], who exposed a series of Au_n nanocrystals to oxidation and found that Au_{55} does not get oxidized under conditions that oxidize bulk Au. These nanocrystals are bequeathed with special stability because they consist of a magic number of metal atoms that enable the complete closure of successive shells of atoms in a cubic close-packed arrangement. The magic numbers 13, 55, 147, 309, and 561 correspond to the closure of 1, 2, 3, 4, and 5 shells, respectively [34]. A schematic illustration of magic nuclearity nanocrystals is shown in Figure 1.2. Since the breakthrough, several magic nuclearity nanocrystals have been prepared including PVP-stabilized Pd_{561} nanocrystals [35]. Figure 1.3, shows scanning tunneling and transmission electron microscopic (TEM) images of polymer-protected Pd_{561} nanocrystals.

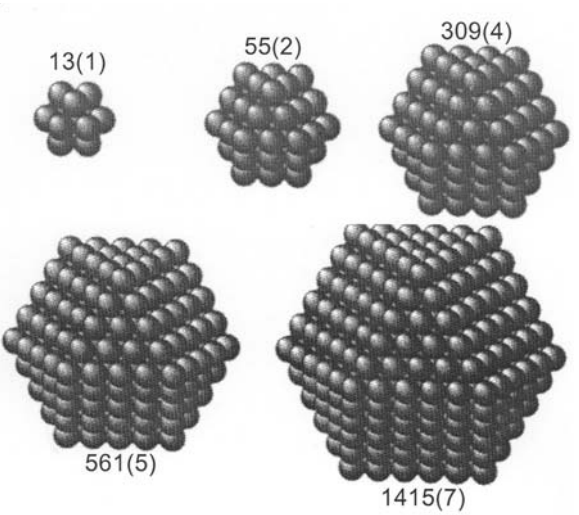

Figure 1.2. Metal nanocrystals in closed-shell configurations with a magic number of atoms. The number of shells is indicated in brackets.

2.3. Shape Control

Since the properties of the nanocrystals follow from the confinement of the electrons to the physical dimensions of the nanocrystals, it would be interesting to vary the shape of the nanocrystals and study the effect of confinement of electrons in such artificial shapes [36]. For example, it is predicted that light emitted from a nanorod would be linearly polarized along the growth axis [37]. Such predictions have led to the revival of interest in synthetic strategies yielding nonspherical nanocrystals. Conventional methods such as those due to Turkevich et al. [13] yield, in addition to spherical particles, a mixture of shapes—triangular, teardrop, and so on—which was then thought of as undesirable. Today, smarter synthetic schemes have been designed which yield selectively nanocrystals in the form of rods, elongated spheres, cubes, and hexagons.

2.4. Tailoring the Ligand Shell

Nanocrystals in their native form are dominated by the surface species, and the capping agents employed play a role in determining the property of the nanocrystals [38]. Hence, in addition to controlling the size and the shape of the nanocrystals, it is also necessary to tailor its surface with the right capping agent. In addition to traditional capping agents that include ions, surfactants,

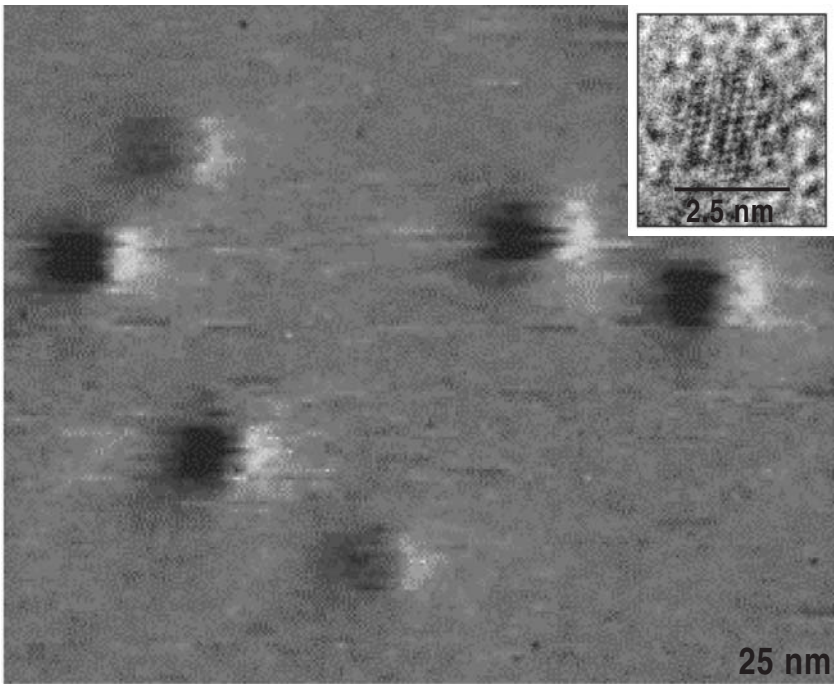

Figure 1.3. Scanning tunneling microscopy image of polymer coated Pd_{561} nanocrystals. The nanocrystals are seen as fluffy balls against plane background of the graphite substrate. The inset shows a high-resolution electron micrograph (HRTEM) of an individual nanocrystal. We see the characteristic 11 [111] fringes in the icosahedral shape measuring 2.5 nm. The diameter estimated from STM is ~3.4 nm, with the difference being due to the ligand shell.

and polymers, a new genre of ligands—dendrimers, hydrogen-bonding fragments of protein, DNA, and dyes—with pendent thiol groups as well as silica layers have been used as capping agents [39–41]. In some cases, a layer of a noble metal is used as a buffer between the core nanocrystal and the ligand shell [42]. Thus, a layer of gold lends special stability to Fe nanocrystals and helps to prevent oxidation and to preserve the magnetic properties of Fe.

Of special interest with regard to tailoring the ligand shells are reactions that enable the total replacement of one set of ligands with another [43–47]. These reactions also typically enable the transfer of nanocrystals from one phase to another. A novel method of thiol-derivatizing hydrosols of metal sols has been developed by Sarathy et al. [44, 45]. The procedure involves mixing vigorously a hydrosol containing metal particles of the desired size distribution

with a toluene solution of an alkane thiol in the presence of a strong acid or reducing agent. The completion of the derivatization is marked by a vivid interchange of the colors from the aqueous layer to the hydrocarbon layer. The advantage of this method is that well-characterized metal particles can be easily thiol-derivatized in a nonaqueous medium. A variety of hydrosols of Au, Ag, and Pt have been thiolized by this procedure.

3. PHYSICAL PROPERTIES OF NANOCRYSTALS

The electronic structure of a nanocrystal critically depends on its very size. For small particles, the electronic energy levels are not continuous as in bulk materials, but discrete, due to the confinement of the electron wavefunction because of the physical dimensions of the particles (see Figure 1.4). The average electronic energy level spacing of successive quantum levels, δ, known as the so-called Kubo gap, is given by

$$\delta = \frac{4E_F}{3n} \tag{1}$$

where E_F is the Fermi energy of the bulk material and n is total number of valence electrons in the nanocrystal. Thus, for an individual silver nanoparticle of 3-nm diameter containing approximately 1000 silver atoms, the value

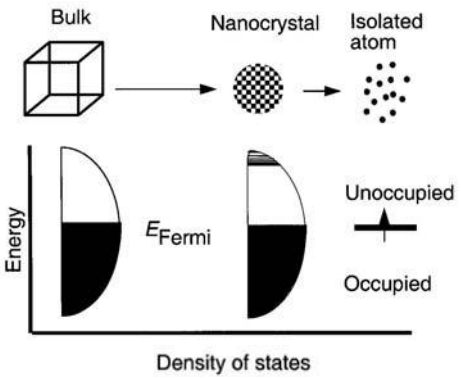

Figure 1.4. Density of states for metal nanocrystals. The density of states is discrete at the band edges. The Fermi level is at the center of a band in a metal, and hence kT exceeds the electronic energy level spacing even at room temperatures and small sizes.

of δ would be 5–10 meV. Since the thermal energy at room temperature, kT, is ~25 meV, a 3-nm particle would be metallic ($kT > \delta$). However, at low temperatures the level spacings, especially in small particles, may become comparable to kT, rendering them nonmetallic [4]. Because of the presence of the Kubo gap in individual nanoparticles, properties such as electrical conductivity and magnetic susceptibility exhibit quantum size effects. The resultant discreteness of energy levels also brings about fundamental changes in the characteristic spectral features of the nanoparticles, especially those related to the valence band.

Extensive investigations of metal nanocrystals of various sizes obtained, for example, by the deposition of metals on amorphized graphite and other substrates, as a result of X-ray photoelectron spectroscopy and related techniques [48–50], have yielded valuable information on their electronic structure. An important result from these experiments is that as the metal particle size decreases, the core-level binding energy of metals such as Au, Ag, Pd, Ni, and Cu increases sharply. This is shown in the case of Pd in Figure 1.5, where the binding energy increases by over 1 eV at small size. The variation in the binding energy is negligible at large coverages or particle size, since the binding energies are close to those of the bulk, macroscopic metals. The increase in the core-level binding energy in small particles occurs due to the poor screening of the core hole and is a manifestation of the size-induced metal–nonmetal transition in nanocrystals. Further evidence for the occurrence of such a metal–nonmetal transition driven by the size of the individual particle is provided by other electron spectroscopic techniques such as UPS and BIS. All these measurements

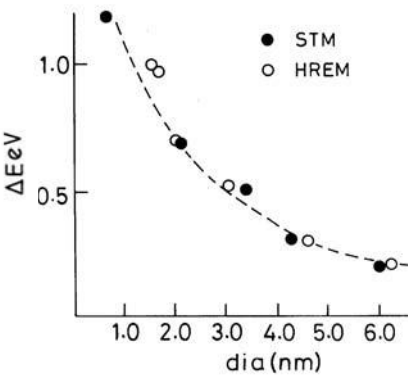

Figure 1.5. Variation of the shift, δE, in the core-level binding energy (relative to the bulk metal value) of Pd with the nanoparticle diameter. The diameters were obtained from HREM and STM images. (Reproduced with permission from reference 50.)

indicate that an electronic gap manifests itself for a nanoparticle with a diameter of 1–2 nm and possessing 300 ± 100 atoms.

Photoelectron spectroscopic measurements [51] on mass-selected Hg_n nanoparticles (n ~ 3–250) in the gas phase reveal that the characteristic HOMO–LUMO (s–p) energy gap decreases gradually from 3.5 eV for $n = 3$ to 0.2 eV for n ~ 250. The band gap closure is predicted at n ~ 400. The metal–nonmetal transition in gaseous Hg nanoparticles was examined by Rademann et al. [52] by measuring the ionization energies (IE). For $n < 13$, the dependence of IE on n suggested a different type of bonding. A small Hg particle with atoms in the $6s^2 6p^0$ configuration held together by relatively weak van der Waals forces, is essentially nonmetallic. As the nanoparticle grows in size, the atomic 6s and 6p levels broaden into bands, and an insulator metal transition appears to occur driven by the physical dimensions of the individual particle. Note that this is the same element, Hg, behaving as either a metal or a nonmetal, depending upon its physical size!

The electronic absorption spectra of metal nanocrystals in the visible region are dominated by the plasmon bands. This absorption is due to the collective excitation of the itinerant electron gas on the particle surface and is characteristic of a nanocrystal of a given size. In metal colloids, surface plasmon excitations impart characteristic colors to the metal sols, with the beautiful wine-red color of gold sols being well known [53–56]. The dependence of the plasmon peak on the dielectric constant of the surrounding medium and the diameter of the nanocrystal was predicted theoretically by Mie and others at the turn of the last century [57–60]. The dependence of the absorption band of thiol-capped Au nanocrystals on solvent refractive index was recently verified by Templeton et al. [61]. Link and El-Sayed [53, 54] found that the absorption band splits into longitudinal and transverse bands in Au nano-rods.

Direct information on the gap states in nanocrystals of metals and semiconductors is obtained by scanning tunneling spectroscopy (STS). This technique provides the desired sensitivity and spatial resolution, making it possible to carry out tunneling spectroscopic measurements on individual particles. A systematic STS study of Pd, Ag, Cd, and Au nanoparticles of varying sizes deposited on a graphite substrate has been carried out under ultrahigh vacuum conditions, after having characterized the nanoparticles by XPS and STM [62]. The I–V spectra of bigger particles were featureless while those of the small particles (<1 nm) showed well-defined peaks on either side of zero bias due to the presence of a gap (see Figure 1.6). It is seen that small particles of ~1-nm diameter are in fact nonmetallic! From the various studies discussed hitherto, it appears that the size-induced metal-insulator transition in metal nanocrystals occurs in the range of 1- to 2-nm diameter or 300 ± 100 atoms.

Theoretical calculations of the electronic structure of metal nanocrystals throw light on the size-induced changes in the electronic structure. Rosenblit

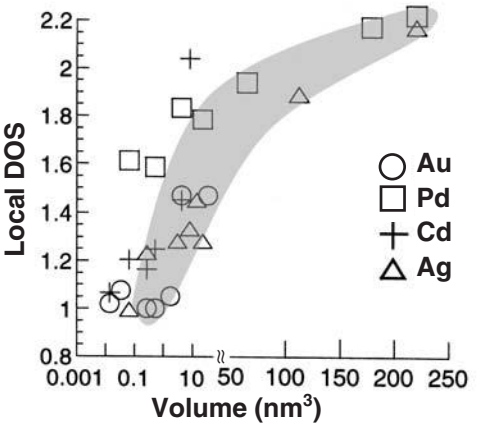

Figure 1.6. Variation of the nonmetallic band gap with nanocrystal volume for various metal nanocrystals, deposited on a graphite surface. The band gaps were estimated by means of scanning tunneling spectroscopy. (Reproduced with permission from reference 62.)

and Jortner [63] calculated the electronic structure of a model metal cluster and predicted electron localization to occur in a cluster of diameter 0.6 nm. A molecular orbital calculation on an Au_{13} cluster [64] in icosahedral and cuboctahedral structures shows that the icosahedral structure undergoes Jahn–Teller distortion while the cuboctahedral structure does not distort. The onset of the metallic state is barely discernible in the Au_{13} cluster. Relativistic density functional calculations of gold clusters [65] with n = 6–147 show that the average interatomic distance increases with the nuclearity of the cluster. The HOMO–LUMO electronic gap decreases with particle size from 1.8 eV for Au_6 (0.5-nm diameter) to 0.3 eV for Au_{147} (2-nm diameter). *Ab initio* molecular dynamics simulations of aluminum clusters [66] with n = 2, 6, 12, 13, 55, and 147 reveal that the minimum energy structures of Al_{13} and Al_{55} are distorted icosahedra whereas Al_{147} is a near-cuboctahedron. The HOMO–LUMO gap increases from 0.5 eV for Al_2 to 2 eV for Al_{13}; the gap is around 0.25 eV for Au_{55} and decreases to 0.1 eV for Au_{147}. The convergence of the cluster properties toward those of the corresponding bulk materials with increase in size is noteworthy.

In a bulk metal, the energy required to add or remove an electron is its work function. In a molecule, the corresponding energies, electron affinity and ionization potential, respectively, are, however, nonequivalent. Because nanocrys-

tals are intermediary, the two energies differ only to a small extent [67], with the difference being the charging energy, U. This is a Coulombic energy and is different from electronic energy gap. Furthermore, Coulombic states can be similar for both semiconductor and metallic nanocrystals, unlike the electronic states. A manifestation of single electron charging is the Coulomb staircase behavior observed in the tunneling spectra [68] when a nanocrystal covered with an insulating ligand shell is held between two tunnel junctions. A typical staircase along with its theoretical fit is shown in Figure 1.7a. Such measurements have also been carried out on Pd and Au nanocrystals in the size range, 1.5 ± 6.5 nm [69]. The charging energies follow a scaling law [70] of the form $U = A + B/d$, where A and B are constants characteristic of the metal and d is the particle diameter (see Figure 1.7b).

Magnetic properties of nanoparticles of transition metals such as Co and Ni show marked variations with size. It is well known that in the nanometric domain, the coercivity of the particles tends to zero [71]. Thus, the nanocrystals behave as superparamagnets with no associated coercivity or retentivity. The blocking temperature that marks the onset of this superparamagnetism also increases with the nanocrystal size. Furthermore, the magnetic moment per atom is seen to increase as the size of a particle decreases [72].

4. CHEMICAL PROPERTIES PROPERTIES OF NANOCRYSTALS

The surface area of nanocrystals increases markedly with the decrease in size. Thus, a small metal nanocrystal of 1-nm diameter will have 100% of its atoms on the surface. A nanocrystal of 10-nm diameter, on the other hand, would have about 15% of its atoms on the surface. A small nanocrystal with a higher surface area would be expected to be more reactive. Furthermore, the qualitative change in the electronic structure arising due to quantum confinement in small nanocrystals will also bestow unusual catalytic properties on these particles, totally different from those of the bulk metal. We illustrate these important aspects with a few examples from the recent literature. A low-temperature study [73] of the interaction of elemental O_2 with Ag nanocrystals of various sizes (Figure 1.8) has revealed the capability of smaller nanocrystals to dissociate dioxygen to atomic oxygen species. On bulk Ag, the adsorbed oxygen species at 80 K is predominantly O^{2-}. This interaction of O_2 with Ag dependent on its particle size is remarkable. Another important example is the reaction of H_2S with Ni nanocrystals giving rise to S^{2-} species, with nanocrystals of different sizes exhibiting different temperature profiles (see Figure 1.9). Unlike bulk nickel, small nanocrystals show less dependence in their catalytic activity on ambient temperature.

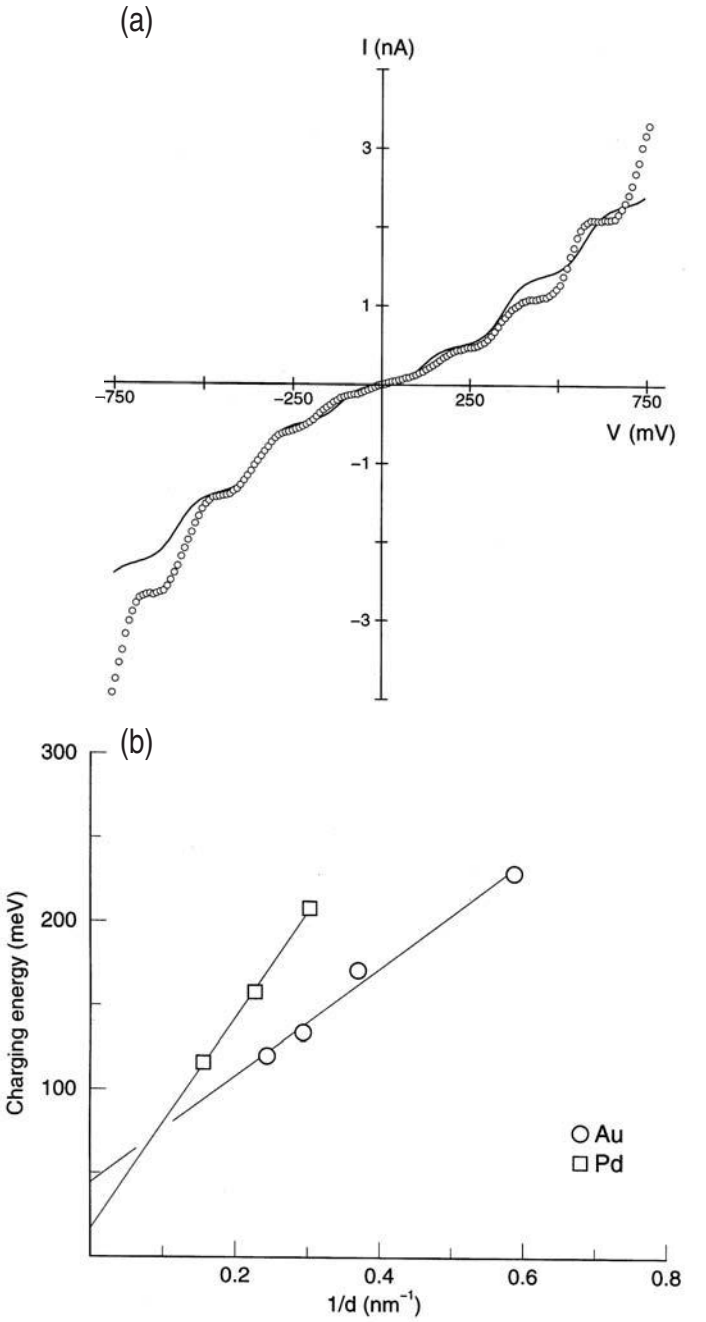

Figure 1.7. (**a**) *I–V* characteristics of an isolated 3.3-nm Pd nanocrystal (dotted line) and the theoretical fit (solid line) obtained at 300 K using a semiclassical model according to which the observed capacitance (C) can be resolved into two components C_1 and C_2, and the resistance (R) can be resolved into R_1 and R_2, such that $C = C_1 + C_2$ and $R = R_1 + R_2$. For $C_1 \ll C_2$ and $R_1 \ll R_2$, the model predicts steps in the measured current to occur at critical voltages, $V_c = n_c e/C + (q_0 + e/2)/C$, where q_0 is the residual charge. (**b**) Variation of the charging energies of Pd and Au nanocrystals with inverse diameters (d). (Reproduced with permission from reference 69.)

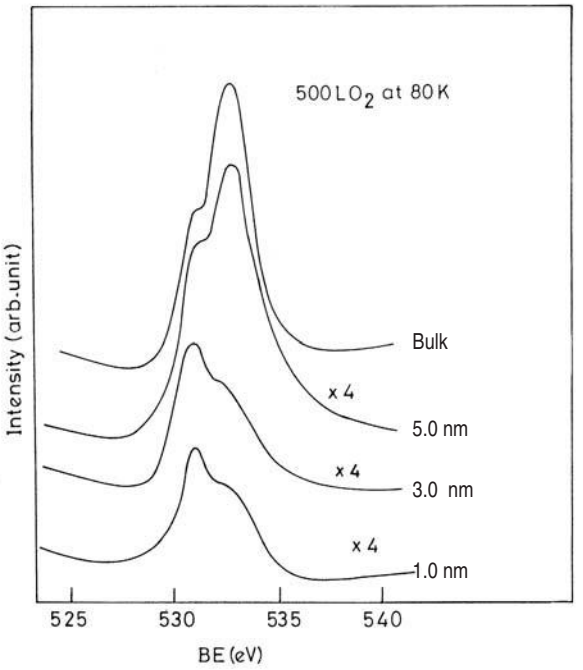

Figure 1.8. Change in the O(1*s*) spectra of Ag clusters exposed to 500 L O_2 at 80 K. The diameters of the clusters were estimated from metal coverage. The lower binding energy peak at 531 eV corresponds to O^- while that at 533 eV arises due to molecular oxygen. (Reproduced with permission from reference 74.)

The ability of Cu, Pd, Pt, and Ni nanoparticles to absorb CO has been thoroughly investigated. Carbon monoxide from a bulk Cu surface desorbs above 250 K. Small Cu particles, however, retain CO up to much higher temperatures [74]. A similar observation has been made in the case of Pd particles [75]. The results obtained with Ni particles are more interesting. In addition to showing a trend similar to the above, small Ni particles are also capable of dissociating CO to form carbidic species on the particle surface (see Figure 1.10) [76]. This could be due to the Ni(3*d*) level in small clusters coming close to the antibonding energy level of CO(2*p**). Heiz and co-workers have studied the ability of a size-selected Pt cluster with nuclearity between 5 and 20 atoms to oxidize CO [77]. The small Pt clusters are all catalytically active and exhibit a different temperature and activity profile, depending on the nuclearity (see Figure 1.11). Simple molecular orbital and geometry-based considerations suffice to describe the catalytic activity in such small clusters [77].

Bulk Au is a noble metal. Goodman and co-workers [78], however, found that Au nanocrystals supported on a titania surface show a marked size effect

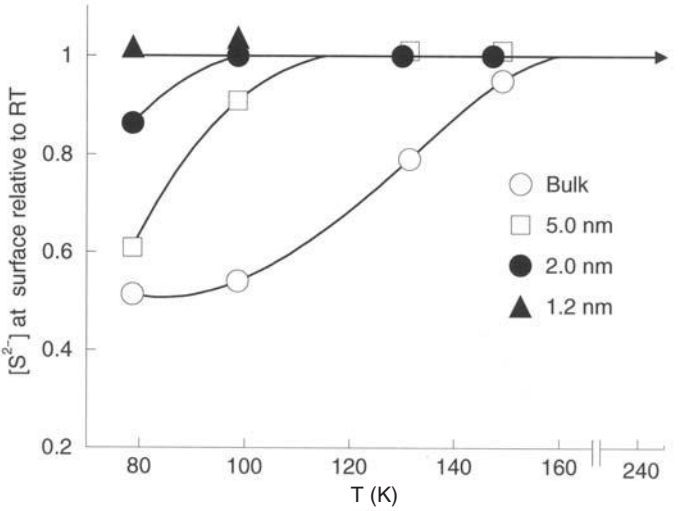

Figure 1.9. Variation of the normalized areas of the signal for the core-level transitions of S^{2-} with temperature for different sizes of Ni clusters deposited on graphite. (Reproduced with permission from reference 73.)

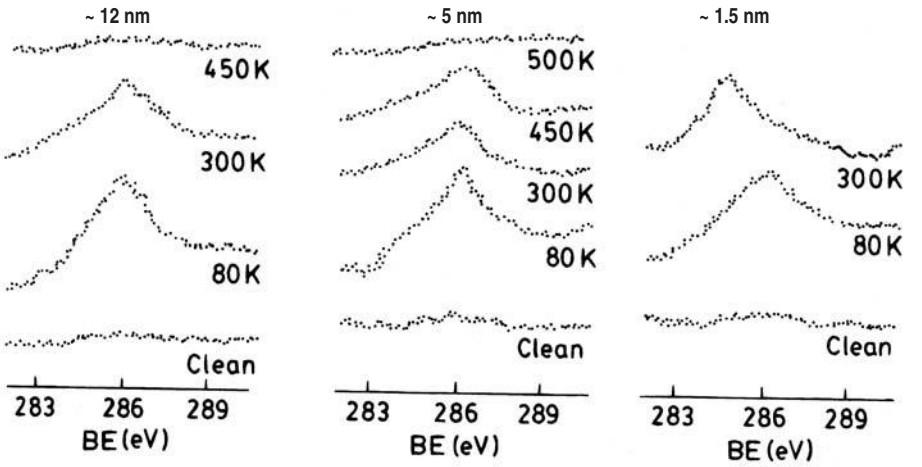

Figure 1.10. Change in the C(1*s*) spectra of CO adsorbed on Ni clusters with temperature. The feature at 286 eV corresponds to molecularly adsorbed CO while that at 284 eV arises due to the formation of carbidic species. (Reproduced with permission from reference 74.)

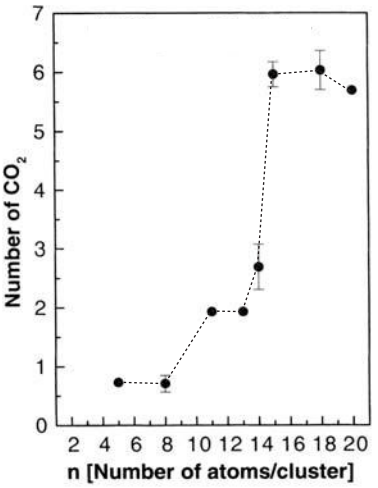

Figure 1.11. A plot of the number of catalytically produced CO_2 molecules against the nuclearity of Pt clusters. The CO_2 molecules produced by oxidation of CO are studied by means of temperature-programmed desorption mass spectrometry. (Reproduced with permission from reference 77.)

in their catalytic ability for CO oxidation reaction, with Au nanoparticles in the range of 3.5 nm exhibiting the maximum chemical reactivity. A metal-to-nonmetal transition was observed in the *I–V* spectra as the cluster size is decreased to below 3.5 nm^3 (consisting of ~300 atoms). This result is quite similar to that obtained with Pd particles supported on oxide substrate [79]. In another study of Au particles supported on a zinc oxide surface, smaller particles (<5 nm) exhibited a marked tendency to adsorb CO while those with diameters above 10 nm did not significantly adsorb CO [80]. Heiz and co-workers have found that small Au clusters (Au_n, $n \leq 20$) exhibit size-dependent catalytic activity above a nuclearity of 8 (see Figure 1.12) [81]. The increased activity of these metal particles is attributed to the charge transfer between the oxide support and the particle surface. It is possible that defects on the oxide surface also play a role in determining the catalytic activity of the nanocrystals.

5. PROGRAMMED ASSEMBLIES

Like molecular systems, nanocrystals capped with suitable ligands spontaneously assemble into ordered aggregates. That such self-assembly can occur through a variety of weak forces is being recognized. Cooperative assemblies of ligated metal and semiconductor and as well as of colloidal polymer spheres

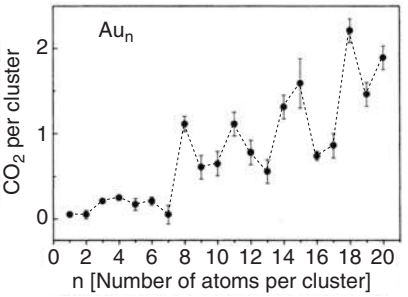

Figure 1.12. A plot of the number of catalytically produced CO_2 molecules against the nuclearity of Au clusters supported on a defect-rich MgO(100) surface. The CO_2 molecules produced by oxidation of CO are studied by means of temperature-programmed desorption mass spectrometry. (Reproduced with permission from reference 81.)

seem to occur through the mediation of electrostatic and capillary forces [67, 82, 83]. The forces that govern the nanocrystal assembly, however, are different in many ways. Surface tension for example, plays an important role [14] because in a nanocrystal a large fraction of atoms are present at the surface. Surfactant molecules that self-assemble on solid surfaces have proved to be the best means of obtaining ordered arrays of nanocrystals [67]. The way in which the nanocrystals organize themselves depends critically on the core diameter, the nature of the ligand, the substrate, and even the dispersive medium used [84]. Thiolized metal nanocrystals readily arrange into two-dimensional arrays on removal of the solvent [6]. Using suitable methods, they can also be put into one-dimensional organization in the form of strings or assembled in a stepwise fashion in a three-dimensional superlattice (see Figure 1.13).

5.1. One-Dimensional Arrangements

Hornayak et al. [85] used the ordered channels of porous alumina as templates to obtain linear arrangements of Au nanocrystals. By varying the pore size, the diameter of the nanowire could be controlled. A linear arrangement has also been obtained by coordinating Au particles (~1.4 nm) stabilized with phosphine ligands to single-stranded DNA oligonucleotide of the desired length and specific sequence [86, 87]. Pt nanocrystals in the form of ribbons has been obtained using a cholesteric liquid crystalline template [88]. Organization of particles in a one-dimensional lattice has met with limited success. Heath and co-workers [89] have fabricated wires of Ag nanocrystals by compressing a dispersion of Ag (4.5 nm) nanocrystals in toluene. The wires were one nanocrystal thick and a few nanocrystals wide, and they extended in length from 20 to 300 nm. The

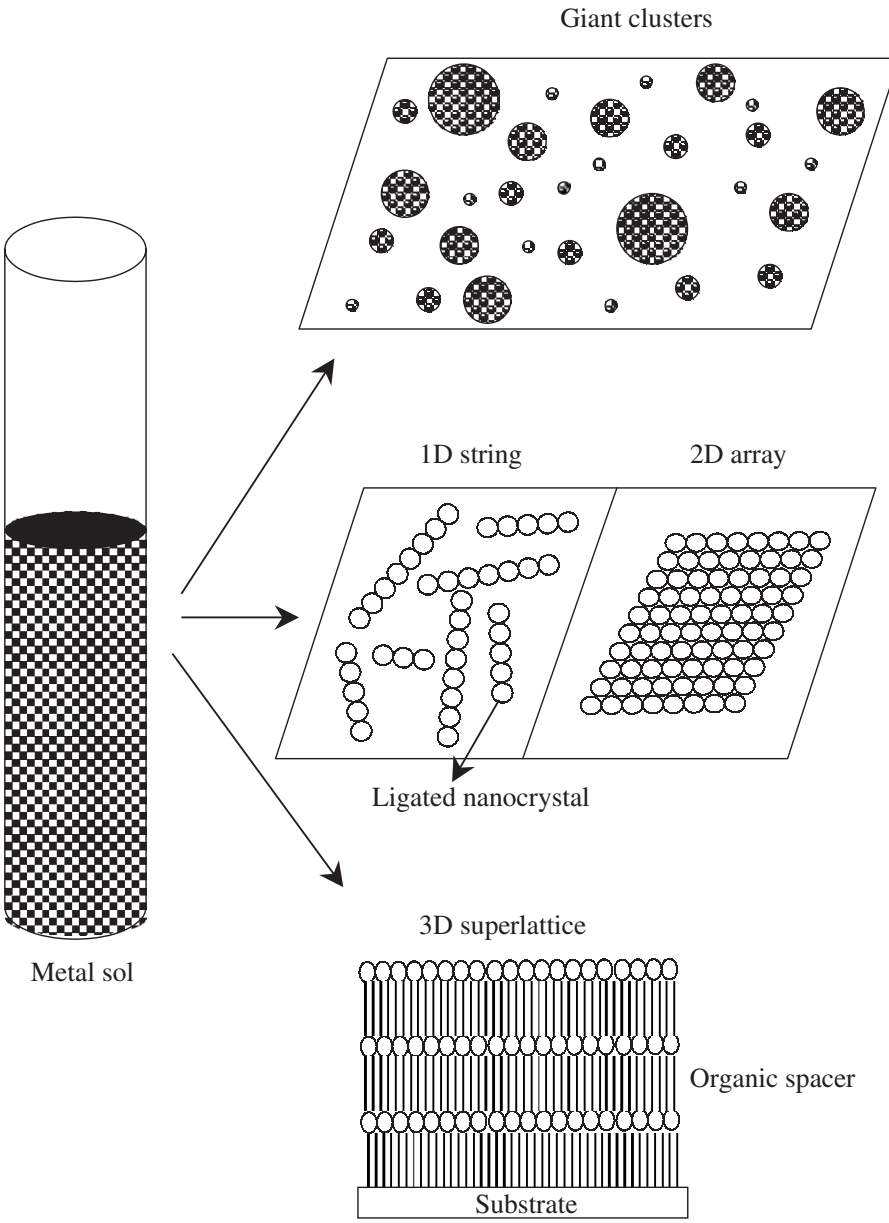

Figure 1.13. Schematic illustration of the various metal nanocrystal organizations.

interwire separation distance as well as the alignment of the wires could be controlled by compressing the film. Based on preliminary experimental observations, it has been suggested tobacco mosaic virus tubules could serve as templates for growth of one-dimensional lattice of quantum dots [90].

5.2. Two-Dimensional Arrays

Ligands based on long-chain thiols or phosphines have served as good candidates for assembling monodisperse nanocrystals on a flat substrate. Two-dimensional organizations of a variety of nanocrystals can be brought about by simply evaporating a drop of the sol on a flat substrate.

Gold organosols using alkane thiols as surfactants were first prepared by Schiffrin and co-workers [91] by phase transferring gold ions and carrying out reduction in the presence of thiols. Several workers have adopted this procedure to obtain thiolized metal nanocrystals [92–95]. Whetten et al. [93] centrifuged the organosol and separated out fractions containing nanocrystals of different mean sizes to prepare well-ordered two-dimensional arrays of size-selected Au nanocrystals. Harfenist et al. [24] found that that Ag nanocrystals prepared by using a cluster beam were stable in air and formed extended two-dimensional arrays. Fitzmaurice and co-workers [94] have obtained two-dimensional arrays of dodecanethiol-covered Ag nanocrystals. The Ag nanocrystals were prepared following the method of Schiffrin and co-workers [91]. Well-ordered arrays of magic nuclearity nanocrystals, Pd_{561} and Pd_{1415}, have been successfully obtained (see Figure 1.14) after replacing their polymer coating by alkanethiols, following the phase transfer method discussed previously [96]. Long-chain fatty acids have also been used for ligating and assembling metal nanocrystals. Colloidal dispersion of Co nanocrystals capped with fatty acids were found to self-assemble to yield hexagonally ordered arrays similar to those obtained with alkanethiols [97, 98]. Similarly, Ag nanocrystals capped with fatty acids of appropriate lengths yield cubic or hexagonal close-packed structures [99, 100]. Schmid et al. [101] have reported an ordered two-dimensional array of small Au_{55} nanocrystals (diameter ~1.4 nm) on a polymer film. At the other end of the size regime, big Au nanocrystals of 15- to 90-nm dimensions have also been organized into two-dimensional arrays [102]. Arrays of Au–Ag [27, 28] and Fe–Pt alloy nanocrystals [26] have been obtained. Magic nuclearity Pd_{561} nanocrystals have been exploited to make Pd–Ni core-shell particles with variable Ni loadings [103]. The nanocrystals so obtained possess a core-shell structure, where an Ni layer covers a Pd seed. The magic nuclearity Pd_{561} nanocrystals act as high-quality seeds and promote the formation of monodisperse Pd–Ni core-nanocrystals. Arrays of $Pd_{561}Ni_n$ (n up to 10,000 atoms) have been prepared after thiolizing the core-shell nanocrystals [104]. By a simple extension of this technique, arrays of triple-layer nanocrystals of the form $Pd_{561}Ni_{3000}Pd_{1500}$ were also obtained. Methods to organize nonspherical metal nanocrystals into two-dimensional arrays have met with very limited success. Thus, hexagonal Pt as well as elongated silver nanocrystals have been organized into ordered two-dimensional arrays [44, 105]. Interestingly, ordered two-dimensional lattices containing thiolized spherical Au particles of two

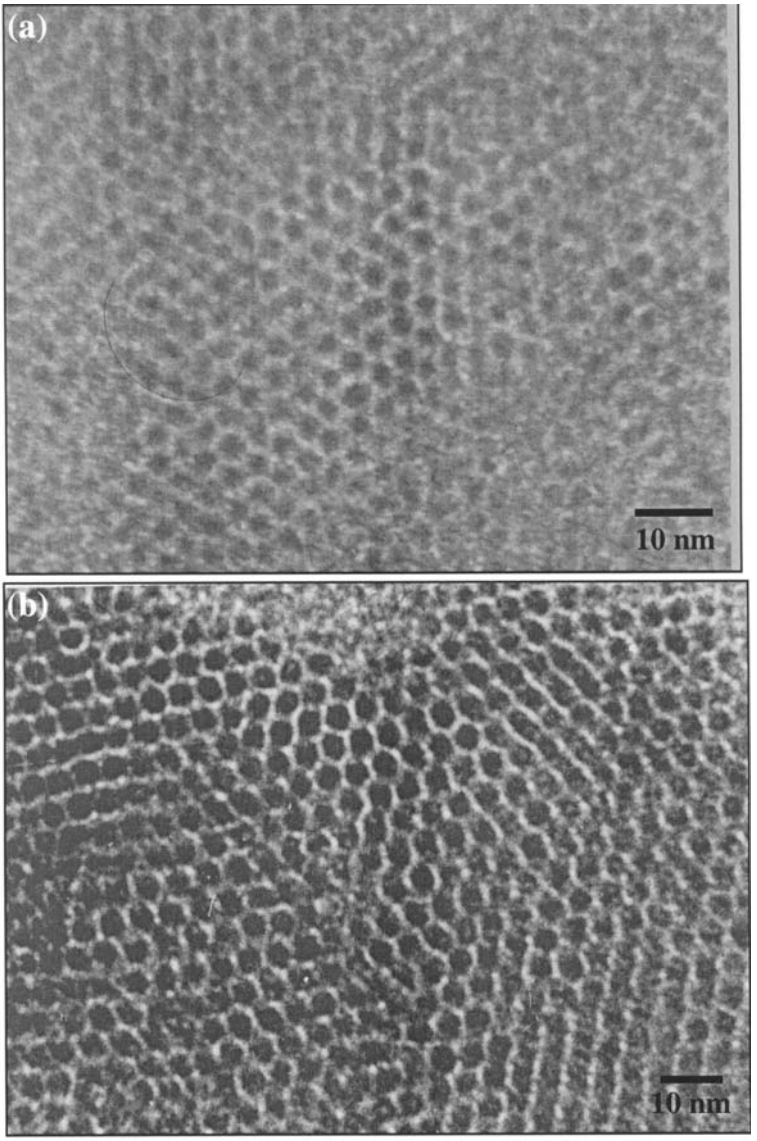

Figure 1.14. TEM micrographs showing hexagonal arrays of thiolized Pd nanocrystals. **(a)** Pd_{561} octanethiol. **(b)** Pd_{1415}, octanethiol. Organized arrays of these nanocrystals extend to lengths over several microns.

different sizes have been reported by Kiely et al. [95], who found that the nanocrystals of different radii follow the radius ratio rules formulated for alloying of different metals. Alloy arrays consisting of Au and Ag nanocrystals of different sizes have been made [106].

5.2.1. Stability and Phase Behavior of Two-Dimensional Arrays. The nanocrystal organizations mentioned above are mainly entropy-driven. The two lengths involved—the nanocrystal diameter (d) and the ligand chain length (l)—play an important role in deciding the nature of the organization—that is, its orderliness. It has been observed experimentally that for a given diameter of the nanocrystal, the packing changes swiftly as the length of the thiol ligand is increased. The stability diagram in terms of d and l shown in Figure 1.15 illustrates that extended close-packed organizations of nanocrystals are found for d/l values ~2. Although entropy-driven, the above cannot be treated as hard-sphere organizations. Based on a study of the effect of the solvent polarity on the self-assembly of ligated metal nanocrystals, Korgel et al. [84, 94] proposed a soft-sphere model taking the interparticle interaction into consideration. Accordingly, a ligated nanocrystal allows for penetration of the ligand shell up to its hard-sphere limit. In this model, the total potential energy, E, is considered to be a result of two types of forces between the nanocrystals:

$$E = E_{\text{steric}} + E_{vdW} \tag{2}$$

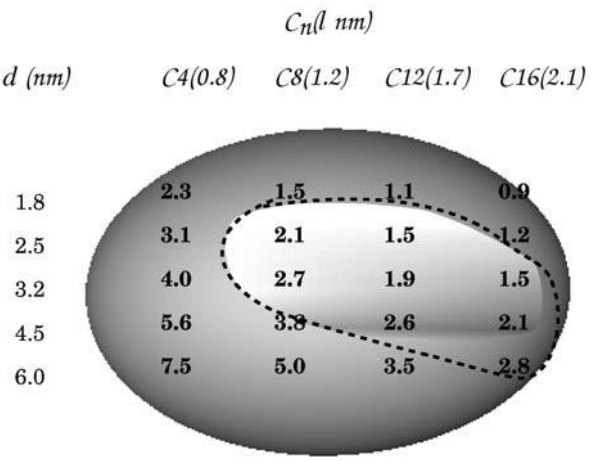

Figure 1.15. The d–l phase diagram for Pd nanocrystals thiolized with different alkanethiols. The mean diameter, d, was obtained from the TEM measurements on as-prepared sols. The length of the thiol, l, is estimated by assuming an all-trans conformation of the alkane chain. The thiol is indicated by the number of carbon atoms, C_n. The bright area in the middle encompasses systems that form close-packed organizations of nanocrystals. The surrounding darker area includes disordered or low-order arrangements of nanocrystals. The area enclosed by the dashed line is derived from calculations from the soft-sphere model.

$$E_{vdW} = \frac{A}{12}\left\{\frac{d^2}{\tau^2 - d^2} + \frac{d^2}{\tau^2} + 2\ln\left[\frac{\tau^2 - d^2}{t^2}\right]\right\} \quad (3)$$

$$E_{\text{steric}} = \frac{50dl^2}{(\tau - d)\pi\sigma_a^3} kTe^{-\pi(\tau - d)} \quad (4)$$

The van der Waals interaction due to the polarization of the metal cores constitutes the attractive term, and the steric interaction between the thiol molecules on the two surfaces forms the repulsive term, where τ is the interparticle distance. The Hamaker constant, A, for Pd nanocrystals, in toluene for instance, has been estimated to be 1.95 eV [107]. The calculated diameter of the area occupied by the thiol molecule (*sa*) on the particle surface is 4.3 Å [94]. The total energy is attractive over a range of interparticle distances, and the magnitude increases with fall in distance. There could be a range of interparticle distances where the attractive energy from the van der Waals term exceeds the repulsive energy due to the steric factor, giving rise to net stabilization of the two-particle system. Stabilization energies of 17 and 2 meV are obtained from the calculation for particles coated with octanethiol and dodecanethiol, respectively. When the stabilization energies have moderate values, comparable to the thermal energy of the nanocrystals, ordered organizations can be expected. If the *d*/*l* and hence the stabilization energy is not favorable, collapsed monolayers of nanocrystals or loosely packed structures are seen. Clearly, the interdigitation of thiol molecules plays a major role in attributing hardness to the ligated nanocrystal, which in turn decides the nature of the two-dimensional organization. A similar treatment should hold good for other nanocrystals.

5.3. Three-Dimensional Superlattices

Multilayer assemblies using monothiols (see Figure 1.13) are generally fragile and are not suited for use in functional devices. One of the means of obtaining robust structures involves multilayer deposition of nanocrystals and has been drawing a great deal of attention over the last few years, since they provide a convenient, low-cost means to prepare ultra-thin films of controlled thicknesses, suited for device applications. In a typical experiment, one end of a monolayer-forming bifunctional spacer is tethered to a flat substrates such as gold, aluminum, indium tin oxide, or glass, leaving the other end free to anchor nanocrystals [6, 7]. Subsequent layers can be introduced by dipping the substrate sequentially into the respective spacer molecule solution and the nanocrystal dispersion, with intermediate steps involving washing and drying. The formation of the multilayer assembly can be monitored using a variety of spectroscopy and microscopy tools. Thus, by employing Au substrates and dithiols as spacers, Sarathy et al. [108] have formed multilayer assemblies of

various nanocrystals. Brust et al. [109] have reported the formation of multilayers of Au nanoparticles using dithiols. These workers have confirmed the layer-by-layer deposition of particle arrays by employing UV-vis spectroscopy and ellipsometry. Three-dimensional superlattices involving nanocrystals of different metals (e.g., Pt and Au) and of metals and semiconductors (e.g., Au and CdS) have also been prepared and characterized [108]. Such assemblies can be made with polyelectrolytes such as poly(diallyldimethylammonium chloride) (PDDA), polyethyleneimine (PEI) [110, 111], and poly(allylamine hydrochloride) (PAH), as well as with polymers such as poly-phenylenevinylene (PPV) [112, 113].

5.4. Giant Nanocrystals

It has been proposed that self-similarity in metal nanocrystal organization would manifest in the form of a giant cluster whose shape and size are direct consequences of the nanocrystals themselves [114]. The invariance of the shell effects in metal nanocrystals with scaling is shown schematically in Figure 1.16.

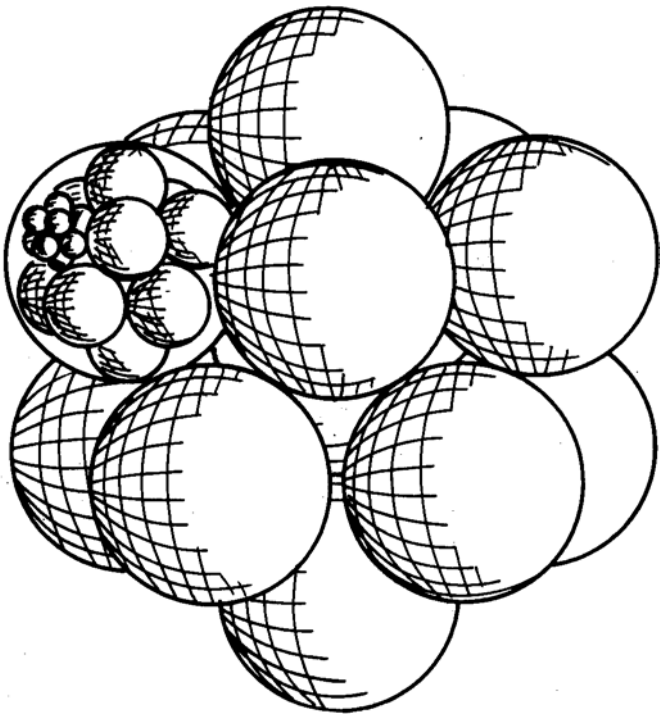

Figure 1.16. Self-similarity. Schematic illustration of the formation of a cluster of metal nanocrystals (super cluster) and a cluster of superclusters. The size effects operating in nanocrystals could be invariant to scaling. (Reproduced with permission from reference 114.)

Thus, Pd_{561} nanocrystals would be expected to self-aggregate into a giant cluster of the type $(Pd_{561})_{561}$ under suitable conditions. The monodisperse nature of the nanocrystals is thought to be important in assisting the self-aggregation process. Formation of such clusters was observed in the mass spectra of magic nuclearity Au_{55} nanocrystals. Secondary ion mass spectrometry indicated the presence of species with large m/z values, and these were attributed to $(Au_{13})_{55}$ giant clusters [115]. However, the giant clusters so obtained have not been isolated or imaged. One such observation was made in the case of Pd_{561} nanocrystals where the PVP-covered nanocrystals aggregated to form giant clusters [116]. The TEM image in Figure 1.17 is revealing. There are regions where the nanocrystals are densely packed in the form of giant aggregates with estimated nanocrystal nuclearities corresponding to various magic numbers. It is possible that the

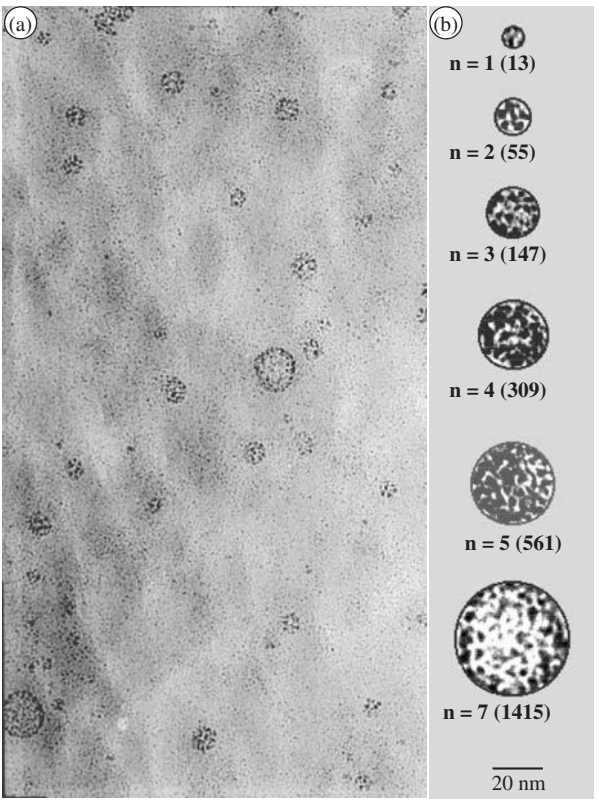

Figure 1.17. (a) TEM micrograph showing the giant clusters comprising Pd_{561} nanocrystals. Sample for TEM was prepared by the slow evaporation of a PVP–Pd_{561} hydrosol. (b) Giant clusters enclosed in circles whose diameters correspond to magic numbers. The n and the values in the parentheses indicate the number of nanocrystals and closed shells, respectively.

formation of the giant clusters is facilitated by the polymer shell that encases them. Unlike in the case of Pd nanocrystals coated with alkanethiols, which self-assemble to form ordered arrays, the polymer shell effectively magnifies the facets of the metallic core, thereby aiding a giant assembly of the nanocrystals.

The tendency of monodisperse nanocrystals to arrange into ordered three-dimensional arrays extending to a few microns has been noticed [117]. Careful tuning of crystallization conditions have yielded crystallites of micrometer dimensions consisting of Au_{55} nanocrystals and Fe–Pt alloy nanocrystals (4.5 nm) [118, 119]. However, it was observed that the nanocrystal arrangement in all the above crystallites was polymorphous. It is believed that such crystallites, consisting of ordered nanocrystals, could prove to be the best candidates to study the collective properties of an ensemble of nanocrystals.

5.5. Nanocrystal Patterning

Creating patterns of nanocrystals on surfaces has attracted wide attention. Such patterned substrates can act as templates to grow nanowires and can serve as etch masks to grow nanopillars and quantum dots [120–122]. Other than the layer-by-layer technique mentioned before, simple techniques such as spin coating have been employed to create a nanocrystalline pattern on surfaces [123]. In the example shown in Figure 1.18, a direct write lithographic technique—dip pen lithography [124, 125]—relies on a cantilever used for atomic force microscopy (AFM) to write on a substrate to create patterns of Au nanocrystals on mica substrates. Thus, nanocrystals of metals and semiconductors can be patterned into rectangles and lines of varying aspect ratios.

6. EMERGING APPLICATIONS

Several applications have been envisaged for nanocrystals, ranging from simple dyes to magnetic-resonance-imaging contrast agents [126], as components of single-electron and nanoscopic electronic circuitry [10, 127], magnetic media [97], as ingredients in catalyst and sensors, and so on. All the above applications seek to exploit the tunability provided by size-dependent properties of the nanocrystals [3].

The dependence of the plasmon band on the dielectric constant of the surrounding medium in metal nanocrystals had been used to detect binding events taking place at the ligand shell. Thus, Au nanocrystals could colorimetrically determine the successful hybridization of oligonucleotide strands bound to its surface [83, 86]. It has been proposed that colorimetric sensing of heavy metal ions could be obtained by the use of carboxylic acid terminated bifunctional

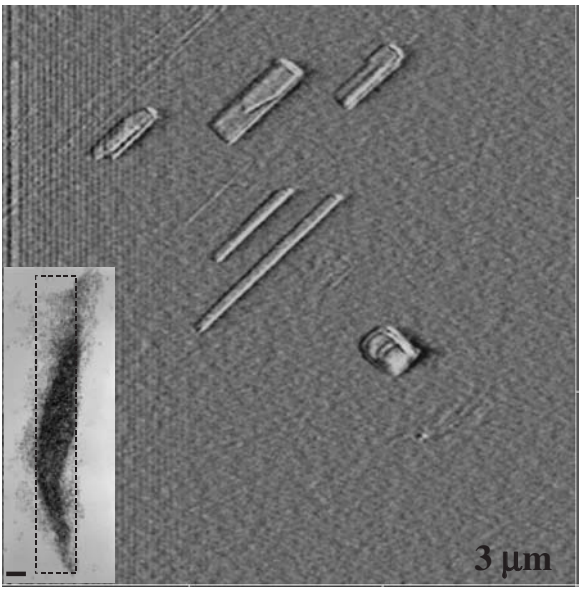

Figure 1.18. Contact AFM scan of a 9-μm^2 area on mica substrate showing rectangles of various aspect ratios filled with Au nanocrystals. The patterns were obtained by translating a AFM cantilever dipped in a sol across the surface. The inset shows a TEM image of a similar pattern on a holey carbon copper grid, and the dotted line bounds the area sought to be filed. The scale bar in the inset corresponds to 50 nm.

thiols bound to metal nanocrystals [128, 129]. The changes in the electronic absorption spectra of ~5-nm Ag nanocrystals capped with lipoic acid, following the addition of the heavy ions Cu^{2+} and Fe^{2+}, are shown in Figure 1.19. Such a dampening also brings about a change in color. It is apparent that Cu^{2+} ions dampen the plasmon band more effectively than Fe^{2+}. It is hoped that mesoscalar organizations could provide useful substrates consisting of ordered nanocrystals that are required to carry out the above experiments in solid state.

The fact that the physical properties of nanocrystal organizations could be different from that of the isolated particles is being realized. Pellets of monodisperse nanocrystals, obtained by the use of bifunctional ligand that binds to more than one nanocrystal or by applying pressure on dried nanocrystalline matter, have been used for electrical transport measurements [130–133]. Pellets made of small Au and Pd nanocrystals exhibit nonmetallic behavior with specific conductivities in the range of $10^6\,\Omega^{-1}\,cm^{-1}$ [130–132]. The conductivity, however, increases dramatically with an increase in the diameter of the nanocrystals. An insulator metal transition has indeed been reported from pellets made of ~12.5-

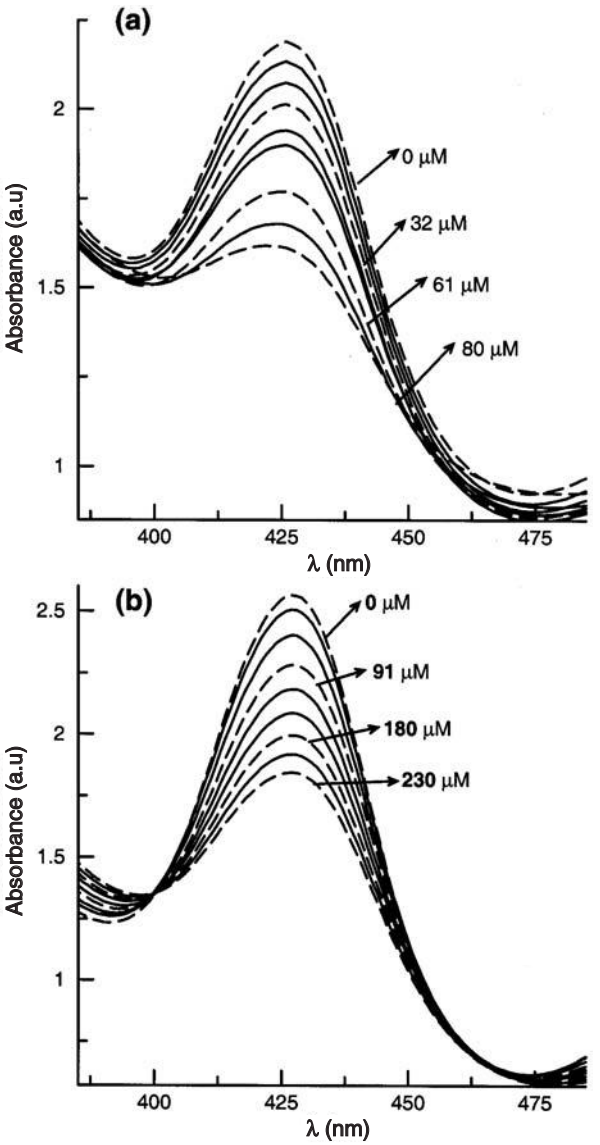

Figure 1.19. Electronic absorption spectra of ~5-nm Ag nanoparticles showing changes accompanying the addition of (**a**) Cu^{2+} and (**b**) Fe^{2+} ions. The concentrations of the ions are indicated. (Reproduced with permission from reference 129.)

nm Au and Ag nanocrystals [133]. Electrical transport measurements on layer-by-layer assemblies of nanocrystals on conducting substrates have been carried out by adoption a sandwich configuration [134–136]. Nanocrystalline films with bulk metallic conductivity have been realized with Au nanocrystals of 5-

and 11-nm diameter spaced with ionic and covalent spacers [135, 136]. The conductivity of a monolayered two-dimensional array of metal nanocrystals has been studied with patterned electrodes [137–142]. Structural disorder and interparticle separation distance are identified as key factors that determine the conductivity of such layers [137–140]. The conductivity of such layers can be enhanced by replacing alkane thiol with an aromatic thiol *in situ* [141, 142]. That the interaction energy of nanocrystals in such organizations can be continually varied by changing the interparticle distance was exploited by Heath and co-workers [143, 144], who prepared a monolayer of Ag (~3 nm) nanocrystals at air–water interface in an LB trough and varied the interparticle distance by applying pressure. A host of measurements including reflectivity and nonlinear optical spectroscopic techniques were carried out *in situ*. This study led to the observation of a reversible Mott–Hubbard metal–insulator transition in the nanocrystal ensemble wherein the Coulomb gap closes at a critical distance between the particles. Tunnelling spectroscopic measurements on films of 2.6-nm Ag nanocrystals capped with decanethiol reveal a Coulomb blockade behavior attributable to isolated nanocrystals [144]. On the other hand, nanocrystals capped with hexane and pentane thiol exhibit characteristics of strong interparticle quantum mechanical exchange. Similar behavior was observed in the case of self-assembled two-dimensional arrays of Co nanocrystals and Au nanocrystals [145, 146].

Alternatives to current magnetic storage media are much sought after. It is believed that arrays of interacting superparamagnetic nanocrystals, whose magnetic properties are governed by the interparticle separation, can be effective alternatives to current hard disks. Nanocrystals of Co, when organized into two-dimensional arrays, exhibit a higher superparamagnetic blocking temperature compared to isolated nanocrystals; that is, they display a higher resistance to thermal reversal of their spins than when they are isolated [147]. Sun et al. report a lattice of nanocrystals, each consisting of an Fe core and a Pt shell prepared by heating Fe–Pt alloy nanocrystals [26]. Following phase segregation, the interaction between the nanocrystals increased, leading to ferromagnetic films capable of supporting high-density magnetization reversal transitions. Exchange spring magnets—nanocomposites that consist of magnetically hard and soft phases interacting via magnetic exchange coupling—have been made by carefully annealing the mixed nanocrystal array consisting of Fe–Pt and Fe_3O_4 [148].

6.1. Nanocomputing

Ordered arrays of nanocrystals, in principle, could be thought of as arrays of SET (single-electron transistors), where the electrostatic interaction between neighboring SET acts as wireless communication means. It has been suggested

by Korotkov [149] and Lent and co-workers [150] that simple logical operations can be performed on a circuitry consisting of arrays of SET in the form of chains or cells with suitable insulating spacers. An electric field applied in one direction polarizes the strings into either the 0 or the 1 state. Lent's scheme, named quantum cellular automata, instead uses a square cell consisting of five nanocrystals to denote the state of polarization. Preliminary experiments to evaluate the schemes are currently being pursued.

The realization that a self-assembly-driven fabrication process is not capable of producing defect free structures has fueled a search for algorithms that can compute even with defective circuitry. Heath et al. [151] have developed Teramac, a computer that works despite a high concentration of defects in its bank of microprocessors. A more radical solution called *amorphous computing* aims to "engineer pre-specified, coherent behavior from cooperation of large numbers of unreliable parts interconnected in unknown, irregular and time-varying ways" [152–154].

7. CONCLUSIONS

Nanocrystals of metal with diameters in the range 1–50 nm form a class of materials with unusual properties that are size-dependent. Excellent electrical conductivity that primarily characterizes a metallic state becomes a rare entity in small nanocrystals (<2 nm) due to quantum confinement of the electronic states. Similarly, magnetic metals lose much of the coercivity with diminishing size. On the other hand, chemical properties such as reactivity may show up better at smaller sizes due to more number of surface bonding sites and other electronic effects. Considering the importance of nanocrystals in technological applications, a large number of synthesis methods have evolved in recent years which include reverse micelle and sonochemical methods besides laser abalation. Control over size and shape as well as encasing the nanocrystals with ligands of specialized functionalities have become subjects of urgent enquiry. While isolated nanocrystals are interesting by themselves, their organizations, especially those that are capable of self-assembling into well-ordered arrays, have attracted greater attention. Nanocrystals anchored to fragments of DNA or likewise molecules essentially form one-dimensional organizations. When coated with long-chain alkane thiols, nanocrystals exhibit a tendency to assemble into hexagonal arrays on flat substrates. The stability of such a two-dimensional organization depends on the diameter of the nanocrystals and the length of the ligand. Multilayers of nanocrystal arrays can also be made in a programmed way by selecting suitable spacer molecules. However, patterns of nanocrystals can be obtained using scanning probe techniques. Another known mesoscalar aggregation is the giant clusters of nanocrystals with

definite nuclearities. It would be ideal to grow crystals of nanocrystals, but such efforts have met with only a limited success to date, giving micron-sized crystals. Nanocrystal organizations may exhibit properties very different from those of the individual. They are amenable to unprecedented control over the lattice, with the size of the nanocrystal and interparticle separation being continuously variable over a range. Exploratory experiments for measuring such collective properties are currently underway in several laboratories around the world.

REFERENCES

1. M. Faraday, *Philos. Trans. R. Soc. London* **147**, 145 (1857).
2. C. R. Berry, *Phys. Rev.* **161**, 848 (1967).
3. C. N. R. Rao, G. U. Kulkarni, P. J. Thomas, and P. P. Edwards, *Chem. Eur. J.* **29**, 27 (2002).
4. P. P. Edwards, R. L. Johnston, and C. N. R. Rao, in *Metal Clusters in Chemistry*, edited by P. Braunstein, G. Oro, and P. R. Raithby, Wiley-VCH, Weinham (1999).
5. R. F. Service, *Science* **274**, 1834 (1996).
6. C. N. R. Rao, G. U. Kulkarni, P. J. Thomas, and P. P. Edwards, *Chem. Soc. Rev.* **29**, 27 (2000).
7. A. N. Shipway, E. Katz, and I. Willner, *CHEMPHYSCHEM* **1**, 18 (2000).
8. M. P. Pileni, *J. Phys. Chem.* **B105**, 3358 (2001).
9. C. B. Murray, C. R. Kagan, and M. G. Bawendi, *Annu. Rev. Mater. Sci.* **30**, 545 (2000).
10. U. Simon, *Adv. Mater.* **10**, 1487 (1998).
11. G. Schmid and L. F. Chi, *Adv. Mater.* **10**, 515 (1998).
12. *Clusters and Colloids: From Theory to Applications*, edited by G. Schmid, VCH, Weinham (1994).
13. J. Turkevich, P. C. Stevenson, and J. Hillier, *J. Discuss. Faraday. Soc.* **11**, 55 (1951).
14. A. I. Kirkland, D. E. Jefferson, D. G. Duff, P. P. Edwards, I. Gameson, B. F. U. Johnson, and D. J. Smith, *Proc. R. Soc. London. A* **440**, 589 (1993).
15. *Physics and Chemistry of Metal Cluster Compounds*, edited by L. J. de Jongh, Kluwer, Dordrecht (1994).
16. T. S. Ahmadi, L. Wang, A. Henglein, and M. A. El-Sayed, *Chem. Mater.* **8**, 428 (1996).
17. M. P. Pileni, *J. Phys. Chem.* **97**, 6961 (1993).
18. I. Moriguchi, F. Shibata, Y. Teraoka, and S. Kagawa, *Chem. Lett.* 761 (1995).
19. M. Platt, R. A. W. Dryfe, and E. P. L. Roberts, *Chem. Commun.* 2324 (2002).
20. C. N. R. Rao, G. U. Kulkarni, P. J. Thomas, V. V. Agrawal, and P. Saravanan, *J. Phys. Chem.* **B107**, 7391 (2003).

21. C. N. R. Rao, G. U. Kulkarni, P. J. Thomas, V. V. Agrawal, U. K. Gautam, and M. Ghosh, *Curr. Sci.* **85**, 1041 (2003).
22. K. Sattler, J. Mhlback, and E. Recknagel, *Phys. Rev. Lett.* **45**, 821 (1980).
23. P. Milani and S. Iannotta, *Cluser Beam Synthesis of Nanostructured Materials*, Springer, Berlin (1999).
24. S. A. Harfenist, Z. L. Wang, R. L. Whetten, I. Vezmar, and M. M. Alvarez, *Adv. Mater.* **9**, 817 (1997).
25. H. N. Vasan and C. N. R. Rao, *J. Mater. Chem.* **5**, 1755 (1995).
26. S. Sun, C. B. Murray, D. Weller, L. Folks, and A. Maser, *Science* **287**, 1989 (2000).
27. N. Sandhyarani, M. R. Reshmi, R. Unnikrishnan, K. Vidyasagar, S. Ma, M. P. Antony, G. P. Selvam, V. Visalakshi, N. Chandrakumar, K. Pandian, Y. T. Tao, and T. Pradeep, *Chem. Mater.* **12**, 104 (2000).
28. S. T. He, S. S. Xie, J. N. Yao, H. J. Gao, and S. J. Pang, *Appl. Phys. Lett.* **81**, 150 (2002).
29. Y.-H. Chen and C.-S. Yeh, *Chem. Commun.* 371 (2001).
30. J.-P. Abid, H. H. Girault, and P. F. Brevet, *Chem. Commun.* 829 (2001).
31. G. Schmid, *Inorg. Synth.* **7**, 214 (1990).
32. M. N. Vargaftik, V. P. Zagorodnikov, I. P. Stolyarov, I. I. Moiseev, V. A. Likholobov, D. I. Kochubey, A. L. Chuvili, V. I. Zaikovsky, K. I. Zamaraev, and G. I. Timofeeva, *Chem. Commun.* 937 (1985).
33. H.-G. Boyen, G. Kastle, F. Weigl, B. Koslowski, C. Dietrich, P. Ziemann, J. P. Spatz, S. Riethmuller, C. Hartmann, M. Moller, G. Schmid, M. G. Garnier, and P. Oelhafen, *Science* **297**, 1533 (2002).
34. T. P. Martin, T. Bergmann, H. Ghlich, and T. Lange, *J. Phys. Chem.* **95**, 6421 (1991).
35. T. Teranishi and M. Miyake, *Chem. Mater.* **10**, 54 (1998); T. Teranishi, H. Hori, and M. Miyake, *J. Phys. Chem.* **B101**, 5774 (1997).
36. S. Link, M. B. Mohamed, and M. A. El-Sayed, *J. Phys. Chem.* **B103**, 3073 (1999).
37. L. Manna, E. C. Scher, and A. P. Alivisatos, *J. Am. Chem. Soc.* **122**, 12700 (2000).
38. P. Zhang and T. K. Sham, *Appl. Phys. Lett.* **81**, 736 (2002).
39. C. M. Niemeyer, *Angew. Chem. Int. Ed.* **40**, 4128 (2001).
40. V. Chechik and R. M. Crooks, *J. Am. Chem. Soc.* **122**, 1243 (2000).
41. P. Mulvaney, L. M. Liz-Marzan, M. Giersig, and T. Long, *J. Mater. Chem.* **10**, 1259 (2002).
42. J. Lin, W. Zhow, A. Kumbhar, J. Wiemann, J. Fang, E. E. Carpenter, and C. J. O'Connor, *J. Solid. State Chem.* **159**, 26 (2001).
43. H. Harai, H. Aizawa, and H. Shiozaki, *Chem. Lett.* **8**, 1527 (1992).
44. K. V. Sarathy, G. Raina, R. T. Yadav, G. U. Kulkarni, and C. N. R. Rao, *J. Phys. Chem.* **B101**, 9876 (1997).
45. K. V. Sarathy, G. U. Kulkarni, and C. N. R. Rao, *Chem. Commun.* 537 (1997).

46. D. I. Gittins and F. Caruso, *Angew. Chem. Int. Ed.* **40**, 3001 (2001).
47. L. O. Brown and J. E. Hutchison, *J. Am. Chem. Soc.* **121**, 882 (1999).
48. (a) D. C. Johnson, R. E. Benfield, P. P. Edwards, W. J. H. Nelson, and M. D. Vargas, *Nature* **314**, 231 (1985); (b) Y. Volokitin, J. Sinzig, L. J. de Jongh, G. Schmid, M. N. Vargaftik, and I. I. Moiseev, *Nature* **384**, 624 (1996).
49. V. Vijayakrishnan, A. Chainani, D. D. Sarma, and C. N. R. Rao, *J. Phys. Chem.* **96**, 8679 (1992).
50. H. N. Aiyer, V. Vijayakrishnan, G. N. Subanna, and C. N. R. Rao, *Surf. Sci.* **313**, 392 (1994).
51. R. Busani, M. Folker, and O. Chesnovsky, *Phys. Rev. Lett.* **81**, 3836 (1998).
52. K. Rademann, O. D. Rademann, M. Schlauf, V. Even, and F. Hensel, *Phys. Rev. Lett.* **69**, 3208 (1992).
53. S. Link and M. A. El-Sayed, *J. Phys. Chem.* **B105**, 1 (2001).
54. S. Link and M. A. El-Sayed, *Int. Rev. Phys. Chem.* **19**, 409 (2001).
55. P. Mulvaney, *Langmuir* **12**, 788 (1996).
56. P. V. Kamat, *J. Phys. Chem.* **B106**, 7729 (2002).
57. G. Mie, *Ann. Phys.* **25**, 377 (1908).
58. G. C. Papavassilliou, *Prog. Solid State Chem.* **12**, 185 (1980).
59. R. Gans, *Ann. Phys.* **31**, 881 (1911).
60. R. Gans, *Ann. Phys.* **47**, 270 (1915).
61. A. C. Templeton, J. J. Pietron, R. W. Murray, and P. Mulvaney, *J. Phys. Chem.* **B104**, 564 (2000).
62. C. P. Vinod, G. U. Kulkarni, and C. N. R. Rao, *Chem. Phys. Lett.* **289**, 329 (1998).
63. M. Rosenblit and J. Jortner, *J. Phys. Chem.* **98**, 9365 (1994).
64. R. A. Perez, A. F. Ramos, and G. L. Malli, *Phys. Rev.* **B39**, 3005 (1989).
65. O. D. Haberlen, S. C. Chung, M. Stener, and N. J. Rosch, *J. Chem. Phys.* **106**, 5189 (1997).
66. S. H. Yang, D. A. Drabold, J. B. Adams, and A. Sachdev, *Phys. Rev.* **B47**, 1567 (1993).
67. C. P. Collier, T. Vossmeyer, and J. R. Heath, *Annu. Rev. Phys. Chem.* **49**, 371 (1998).
68. *Single Charge Tunneling*, *Coulomb Blockade Phenomena in Nanostructures,* edited by H. Grabert and M. H. Devoret, NATO-ASI Ser. B (1992), p. 294.
69. P. J. Thomas, G. U. Kulkarni, and C. N. R. Rao, *Chem. Phys. Lett.* **321**, 163 (2000).
70. J. Jortner, *Z. Phys. D: Atoms, Molecules and Clusters* **24**, 247 (1992).
71. C. P. Bean and J. D. Livingston, *J. Appl. Phys.* **30**, 1208 (1959).
72. Van de Heer, P. Milani, and A. Chatelain, *Z. Phys. D: Atoms, Molecules and Clusters* **19**, 241 (1991).
73. C. N. R. Rao, V. Vijayakrishnan, A. K. Santra, and M. W. J. Prins, *Angew. Chem. Int. Ed.* **31**, 1062 (1992).

74. A. K. Santra, S. Ghosh, and C. N. R. Rao, *Langmuir* **10**, 3937 (1994).
75. E. Gillet, S. Channakhone, V. Matolin, and M. Gillet, *Surf. Sci.* **152/153**, 603 (1986).
76. (a) D. L. Doering, J. T. Dickinson, and H. Poppa, *J. Catal.* **73**, 91 (1982); (b) D. L. Doering, H. Poppa, and J. T. Dickinson, *J. Catal.* **73**, 104 (1982).
77. U. Heiz, A. Sanchez, S. Abbet, and W.-D. Schneider, *J. Am. Chem. Soc.* **121**, 3214 (1999).
78. M. Valden, X. Lai, and D. W. Goodman, *Science* **281**, 1647 (1998).
79. C. Xu, X. Lai, G. W. Zajac, and D. W. Goodman, *Phys. Rev.* **56**, 13464 (1997).
80. C. P. Vinod, G. U. Kulkarni, and C. N. R. Rao, in *Surface Chemistry and Catalysis*, edited by A. Carley, P. Davies, G. Hutchings, and M. Spencer, Kluwer Academic/Plenum Publishers (2003).
81. A. Sanchez, S. Abbet, U. Heiz, W.-D. Schneider, H. Häkkinen, R. N. Narnett, and U. Landman, *J. Phys. Chem.* **103**, 9573 (1999).
82. A. Terfort, N. Bowden, and G. M. Whitesides, *Nature* **386**, 162 (1997).
83. C. A. Mirkin, R. L. Letsinger, R. C. Mucic, and J. F. Storhoff, *Nature* **382**, 607 (1996).
84. B. A. Korgel and D. Fitzmaurice, *Phys. Rev. Lett.* **80**, 3531 (1998).
85. G. L. Hornayak, M. Krll, R. Pugin, T. Sawitowski, G. Schmid, J. O. Bovin, G. Karrson, H. Hofmeister, and S. Hopfe, *Eur. J. Chem.* **3**, 195 (1997).
86. A. P. Alivisatos, K. P. Johnsson, X. Peng, T. E. Wilson, C. J. Loweth, M. P. Jr. Burchez, and P. G. Schultz, *Nature* **382**, 609 (1996).
87. A. Kumar, M. Pattarkine, M. Bhadbhade, A. B. Mandale, K. N. Ganesh, S. S. Datar, C. V. Dharmadhikari, and M. Sastry, *Adv. Mater.* **13**, 341 (2001).
88. S.-W. Lee, C. Mao, C. E. Flynn, and A. M. Belchar, *Science* **296**, 892 (2002).
89. S. W. Chung, G. Markovich, and J. R. Heath, *J. Phys. Chem.* **B102**, 6685 (1998).
90. E. Dujardin, C. Peet, G. Stubbs, J. N. Culver, and S. Mann, *Nano Lett.* **3**, 413 (2003).
91. M. Brust, M. Walker, D. Bethell, J. D. Schiffrin, and R. Whyman, *Chem. Commun.* 801 (1994).
92. N. Sandhyarani and T. Pradeep, *Chem. Mater.* **12**, 1755 (2000).
93. R. L. Whetten, J. T. Khoury, M. M. Alvarez, S. Murthy, I. Vezmar, Z. Wang, P. W. Stephens, C. L. Clevend, W. D. Luedtke, and U. Landman, *Adv. Mater.* **8**, 428 (1996).
94. B. A. Korgel, S. Fullam, S. Connolly, and D. Fitzmaurice, *J. Phys. Chem.* **B102**, 8379 (1998).
95. C. J. Kiely, J. Fink, M. Brust, D. Bethell, and D. J. Schiffrin, *Nature* **396**, 444 (1998).
96. P. J. Thomas, G. U. Kulkarni, and C. N. R. Rao, *J. Phys. Chem.* **B104**, 8138 (2000).
97. S. Sun and C. B. Murray, *J. Appl. Phys.* **85**, 4325 (1999).

98. C. Petit, A. Taleb, and M. P. Pileni, *J. Phys. Chem.* **B103**, 1805 (1999).
99. M. P. Pileni, *New J. Chem.* 693 (1998).
100. K. Abe, T. Hanada, Y. Yoshida, N. Tanigaki, H. Takiguchi, H. Nagasawa, M. Nakamoto, T. Yamaguchi, and K. Yase, *Thin Solid Films* **327–329**, 524 (1998).
101. G. Schmid, M. Bäumle, and N. Beyer, *Angew. Chem. Int. Ed.* **1**, 39 (2000).
102. B. Kim, S. L. Tripp, and A. Wei, *J. Am. Chem. Soc.* **123**, 7955 (2001).
103. T. Teranishi and M. Miyake, *Chem. Mater.* **11**, 3414 (1999).
104. P. J. Thomas, G. U. Kulkarni, and C. N. R. Rao, *J. Nanosci. Nanotechnol.* **1**, 267 (2001).
105. B. A. Korgel and D. Fitzmaurice, *Adv. Mater.* **10**, 661 (1998).
106. C. J. Kiely, J. Fink, J. G. Zheng, M. Brust, D. Bethell, and D. J. Schiffrin, *Adv. Mater.* **12**, 639 (2000).
107. D. Bargeman and F. V. V. Vader, *J. Electroanal. Chem.* **37**, 45 (1972).
108. K. V. Sarathy, P. J. Thomas, G. U. Kulkarni, and C. N. R. Rao, *J. Phys. Chem.* **B103**, 399 (1999).
109. M. Brust, D. Bethell, C. J. Kiely, and D. J. Schiffrin, *Langmuir* **14**, 5425 (1998).
110. R. Blonder, L. Sheeney, and I. Willner. *Chem. Commun.* 1393 (1998).
111. Y. Liu, Y. Wany, and R. O. Claus, *Chem. Phys. Lett.* **298**, 315 (1998).
112. A. Samokhvalov, M. Berfeld, M. Lahav, R. Naaman, and E. Rabani, *J. Phys. Chem.* **B104**, 8632 (2000).
113. M. Gao, B. Richter, and S. Kirstein, *Adv. Mater.* **9**, 802 (1997).
114. H. G. Fritsche, H. Muller, and B. Fehrensen, *Z. Phy. Chem.* **199**, 87 (1997).
115. H. Feld, A. Leute, D. Rading, A. Benninghoven, and G. Schmid, *J. Am. Chem. Soc.* **112**, 8166 (1990).
116. P. J. Thomas, G. U. Kulkarni, and C. N. R. Rao, *J. Phys. Chem.* **B105**, 2515 (2001).
117. M. Maillard, L. Motte, A. T. Ngo, and M. P. Pileni, *J. Phys. Chem.* **B104**, 11871 (2000).
118. G. Schmid, R. Pugin, T. Sawitowski, U. Simon, and B. Marler, *Chem. Commun.* 1303 (1999).
119. E. Shevchenko, D. Talapin, A. Kornowski, F. Wiekhorst, J. Kötzler, M. Haase, A. Rogach, and H. Weller, *Adv. Mater.* **14**, 287 (2002).
120. H. Ago, T. Komatsu, S. Ohshima, Y. Kuriki, and M. Yumura, *Appl. Phys. Lett.* **77**, 79 (2000).
121. Y. Cui, L. J. Lauhon, M. S. Gudisksen, J. Wang, and C. M. Lieber, *Appl. Phys. Lett.* **78**, 2214 (2001).
122. P. A. Lewis, H. Ahamed, and T. Sato, *J. Vac. Sci. Technol.* **B16**, 2938 (1998).
123. Y.-K. Hong, H. Kim, G. Lee, W. Kim, J. Park, J. Cheon, and J.-Y. Koo, *Appl. Phys. Lett.* **80**, 844 (2002).
124. R. D. Piner, J. Zhu, F. Xu, S. Hong, and C. A. Mirkin, *Science* **283**, 661 (1999).
125. C. A. Mirkin, S. Hong, and L. Demers, *Chem. Phys. Chem.* **2**, 37 (2001).

126. C. R. Martin and D. T. Mitchell, *Anal. Chem.* 322A (1998).
127. D. L. Feldheim and C. D. Keating, *Chem. Soc. Rev.* **27**, 1 (1998).
128. Y. Kim, R. C. Johnson, and J. T. Hupp, *Nano Lett.* **1**, 165 (2001).
129. S. Berchmans, P. J. Thomas, and C. N. R. Rao, *J. Phys. Chem.* **B106**, 4651 (2002).
130. M. Brust, D. Bethell, D. J. Schiffrin, and C. J. Kiely, *Adv. Mater.* **7**, 795 (1995).
131. V. Torma, G. Schmid, and U. Simon, *Chem. Phys. Chem.* **1**, 321 (2001).
132. U. Simon, R. Flesch, H. Wiggers, G. Schn, and G. Schmid, *J. Mater. Chem.* **8**, 517 (1998).
133. M. Aslam, I. S. Mulla, and K. Vijayamohanan, *Appl. Phys. Lett.* **79**, 689 (2001).
134. R. H. Terrill, T. A. Postlewaite, C. Chen, C. D. Poon, A. Terzis, A. Chen, J. E. Hutchinson, M. R. Clark, G. Wignall, J. D. Londono, R. Superfine, M. Falvo, C. S. Johnson, Jr., E. T. Samulski, and R. W. Murray, *J. Am. Chem. Soc.* **117**, 1237 (1995).
135. M. D. Musick, C. D. Keating, M. H. Keefe, and M. J. Natan, *Chem. Mater.* **9**, 1499 (1997).
136. Y. Liu, Y. Wang, and R. O. Clauss, *Chem. Phys. Lett.* **298**, 315 (1998).
137. R. Parthasarathy, X.-M. Lin, and H. A. Jaeger, *Phys. Rev. Lett.* **87**, 186807 (2001).
138. J. Schmelzer, Jr., S. A. Brown, A. Wurl, H. Hyslop, and R. J. Blaikie, *Phys. Rev. Lett.* **88**, 226802 (2002).
139. R. C. Doty, H. Yu, C. K. Shih, and B. A. Korgel, *J. Phys. Chem.* **B105**, 8291 (2001).
140. T. Ogawa, K. Kobayashi, G. Masuda, T. Takase, and S. Maeda, *Thin Solid Films* **393**, 374 (2001).
141. R. G. Osifchin, W. J. Mahoney, J. D. Bielefeld, R. P. Andres, J. I. Henderson, and C. P. Kubiak, *Superlattices and Microstructures* **18**, 283 (1995).
142. R. G. Osifchin, W. J. Mahoney, J. D. Bielefeld, R. P. Andres, J. I. Henderson, and C. P. Kubiak, *Superlattices and Microstructures* **18**, 275 (1995).
143. G. Markovich, C. P. Collier, S. E. Hendricks, F. Ramacle, R. D. Levine, and J. R. Heath, *Acc. Chem. Res.* **32**, 415 (1999).
144. G. Medeiros-Ribeiro, D. A. A. Ohlberg, R. S. Williams, and J. R. Heath, *Phys. Rev.* **B59**, 1633 (1999).
145. A. Taleb, F. Silly, A. O. Gusev, F. Charra, and M.-P. Pileni, *Adv. Mater.* **12**, 633 (2000).
146. T. P. Bigioni, L. E. Harrell, W. G. Cullen, D. K. Guthrie, R. L. Whetten, and P. N. Fist, *Eur. Phys. J.* **D6**, 355 (1999).
147. V. Russier, C. Petit, J. Legrand, and M. P. Pileni, *Phys. Rev.* **B62**, 3910 (2000).
148. H. Zheng, J. Li, J. P. Llu, Z. L. Whang, and S. Sun, *Nature* **420**, 395 (2002).
149. *Molecular Electronics*, IUPAC "Chemistry for the 21st Century" monograph, edited by J. Jortner and M. Ratner, Blackwell Scientific, London (1997).
150. A. O. Orlov, I. Amlani, G. H. Berstein, C. S. Lent, and G. L. Snider, *Science* **277**, 928 (1997).

151. J. R. Heath, P. J. Kuekes, G. S. Snider, and R. S. Williams, *Science* **280**, 1717 (1998).

152. H. Abelson, D. Allen, D. Coore, C. Hanson, G. Homsy, T. F. Knoght, Jr., R. Nagpal, E. Rauch, G. J. Sussman, and R. Weiss, Technical Report A. I. Memo 1665, Massachusetts Institute of Technology, Artificial Intelligence Laboratory, Aug. 1999.

153. D. Coore, R. Nagpal, and R. Weiss, Technical Report A. I. Memo 1614, Massachusetts Institute of Technology, Artificial Intelligence Laboratory, Oct. 1997.

154. H. Abelson, D. Allen, D. Coore, C. Hanson, G. Homsy, T. F. Knoght, Jr., R. Nagpal, E. Rauch, G. J. Sussman, and R. Weiss, *Commun. Assoc. Comp. Mach.* **43**, 5 (2000).